SigCan: Toward Reliable ToF Estimation Leveraging Multipath Signal Cancellation on Commodity WiFi Devices

Yang Li, Dan Wu, Jiahe Chen, Weiyan Shi, Leye Wang, *Member, IEEE*, Lu Su, *Member, IEEE*, Wenwei Li, and Daqing Zhang, *Fellow, IEEE*

***Abstract*—The widespread deployment of WiFi infrastructure has facilitated the development of Time-of-Flight (ToF) based sensing applications. ToF estimation, however, is a challenging task due to the complexity of multipath effect. In this paper, we propose a phase difference based method for ToF estimation and uncover the potential of signal cancellation to mitigate the impact of multipath and noise on phase differences among subcarriers. To separate the moving target path from the complex multipath for ToF estimation, we suggest employing specific elimination methods tailored to the characteristics of different signal components. For dynamic multipath, we observe that when a given subcarrier propagates along two paths to the receiver, with path lengths differing by half a wavelength, the phase difference introduced by these two paths cancels each other out. Therefore, we propose two metrics to identify signals that satisfy this condition, utilizing both frequency diversity and spatial diversity. Additionally, we propose leveraging time diversity to eliminate the static multipath component and reduce the impact of noise. We implemented the methods with off-the-shelf WiFi devices and achieved mean errors of 15.36 cm and 21.05 cm for distance estimation in outdoor and indoor scenarios, outperforming state-of-the-art ToF estimation method by 50% error reduction.**

***Index Terms*—Channel State Information (CSI), Time of Flight (ToF), Wireless Sensing.**

I. Introduction

TIME-OF-FLIGHT (ToF) represents the time it takes for a signal to propagate through a channel from the transmitter to the receiver. It plays a crucial role in WiFi sensing applications, which has garnered the interest of many researchers [1], [2]. ToF can be measured by directly detecting signals with different arrival times in the time domain, e.g., Round Trip Time (RTT) based method. However, this method necessitates specialized hardware with high signal sampling frequencies [3], [4], [5], [6].

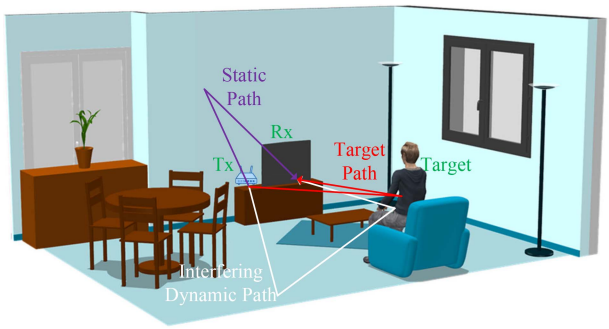

Fig. 1. Obtaining the ToF introduced by the target serves many applicants, which is challenging due to the multipath in the real world.

An alternative approach to measure the ToF is by using Channel State Information (CSI), which can be acquired from widely available WiFi network interface cards (NICs), such as Intel 5300, Atheros 9580, etc. Theoretically, in cases where only a single propagation path exists in the environment, it is relatively straightforward to use Inverse Fast Fourier Transform (IFFT) to find the time delay at which the signal reaches the receiver via that path. However, in real-world indoor environments such as the one shown in Fig. 1, signals arrive at the receiver through multiple propagation paths. Among these, the paths where the signal reaches the receiver in a single reflection via the monitored target (e.g., a human subject as shown in Fig. 1) are referred to as the target path, (i.e., red line). Some of the signals reach the receiver through either the direct line-of-sight path or reflections on static objects, such as walls, so their propagation paths' lengths remain constant over time. We refer to these paths as static paths, (i.e., purple line). Another portion of the signals reach the receiver after multiple reflections off not only the moving target but also the ambient objects. These signals, being affected by the movement of the target, would cause interference in the estimation of the target's ToF. For this reason, we

Received 21 December 2023; revised 10 October 2024; accepted 23 October 2024. Date of publication 4 November 2024; date of current version 5 February 2025. This work was supported by NSFC A3 Project under Grant 62061146001, and in part by PKU-NTU Collaboration Project. Recommended for acceptance by X. Tian. *(Corresponding author: Daqing Zhang.)*

Yang Li, Dan Wu, Leye Wang, and Wenwei Li are with the School of Computer Science, Peking University, Beijing 100871, China (e-mail: liyang@stu.pku.edu.cn).

Jiahe Chen is with the School of Electronics Engineering and Computer Science, Peking University, Beijing 100871, China.

Weiyan Shi is with the School of Software and Microelectronics, Peking University, Beijing 100871, China.

Lu Su is with the School of Electrical and Computer Engineering, Purdue University, West Lafayette, IN 47907 USA.

Daqing Zhang is with the Key Lab of High Confidence Software Technologies, Ministry of Education, Peking University, Beijing 100871, China, also with the School of Computer Science,Peking University, Beijing 100871, China, and also with SAMOVAR Lab, IP Paris, Evry, Telecom SudParis, 91000 Fourier, France (e-mail: dqzhang@sei.pku.edu.cn).

Digital Object Identifier 10.1109/TMC.2024.3491337

refer to these paths as interfering dynamic paths, (i.e., white line). The aforementioned static paths and interfering dynamic paths make it challenging to discern the ToF of the target path.

To distinguish the delay introduced by the target path amidst multiple paths, one approach is to enlarge the bandwidth used for estimation. A larger bandwidth results in an enhanced capability to differentiate ToF values across multiple paths. Previous work [7] achieves nearly 1 Gbps bandwidth by combining multiple channels within the 2.4G and 5G spectra, obtaining a resolution of decimeters. However, this approach is incompatible with current WiFi protocols and requires hardware and software modifications. Another type of approaches [8], [9], [10], [11], distinguishes multiple paths by utilizing multiple dimensions of parameters, including ToF, Angle of Arrival (AoA), Doppler Frequency Shift (DFS), and Angle of Departure (AoD) to improve multipath discrimination. When bandwidth limitations lead to low ToF distance precision, if these signals arrive at the receiver with large incidence angle differences, they can be distinguished through the AoA dimension. However, due to the fact that the polarization direction and installation position of many WiFi devices have not been designed to meet the requirements for calculating the AoA, deriving accurate AoA information can be challenging for some devices. In order to enable the ToF-based application to existing WiFi devices in real-world environments, it is preferable to reuse the channels provided by the existing WiFi protocol, which limits the available bandwidth. And we have to leverage the CSI collected with randomly positioned antennas. These constraints compel us to seek new methods for ToF estimation.

We delve into utilizing the phase of the frequency-domain CSI for ToF estimation. The fundamental principle of ToF estimation is that the phase difference of signals collected on two subcarriers with a small frequency difference changes proportionally to the path length over a large area. However, it is a challenging task to extract the cross-subcarrier phase differences introduced by the target path from the superimposed signals of multiple paths. To address this challenge, we propose a **Signal Cancellation** based framework (SigCan) and explore its potential to mitigate the impact of multipath and noise on phase differences. We also develop a series of novel mechanisms based on the characteristics of different multipath components, progressively eliminating the impact of multipath on the extraction of the target path's phase differences.

We start with elimination of static paths. Since the lengths of static paths do not change over time, the signal phases introduced by them remain constant. Therefore, by taking the difference between signal samples at closely adjacent instants, static multipath components in the signal can be canceled out, preserving the phase difference introduced by the dynamic paths.

As for the interfering dynamic paths, we envision that some of them may cancel each other in specific conditions so that they will not affect the phase difference introduced by the target path. Such an insight comes from the observation that when a WiFi signal with a given wavelength propagates through two dynamic paths with a path length difference of half a wavelength, the signal variation caused by these two paths nullifies each other at the receiver. We hypothesize that such a cancellation condition can be found through exploring spatial diversity and frequency diversity since the disparity in position/wavelength introduces abundant superpositions of interfering dynamic paths.

Now the question is how to identify the signals experiencing multipath cancellation. We have observed that once the effects of multipath are nullified, the signal variation is mainly influenced by the target path. Therefore, for a given time, the phases of different subcarriers should exhibit a linear relationship, and the signal patterns of different subcarriers closely resemble each other. Therefore, we can identify whether signals have dynamic multipath cancellation based on the linear relationship of phases among different subcarriers and the similarity of signal patterns.

Besides the multipath, signal noise would also exert an influence on phase differences introduced by the target path. Since the ambient noise follows an independent Gaussian distribution [12], we designed an algorithm that employs signal samples over a relatively long period of time to calculate phase differences on the complex plane, reducing the impact of noises. In summary, our contributions can be summarized as follows:

1) We propose a novel phase difference based method for ToF estimation and uncover the potential of signal cancellation to mitigate the impact of multipath and noise on phase differences of the target path.
2) To tackle the multipath issues, we suggest employing specific elimination methods tailored to the characteristics of different signal components. Specifically, for the most challenging interfering dynamic multipath, we introduced metrics for the first time to quantify the extent of interfering dynamic multipath cancellation. With these metrics, we can identify signals that are unaffected by the interference of dynamic paths, and extract phase difference for reliable ToF estimation.
3) To implement the above idea, we have designed a framework to mitigate the influence of multipath and noise on the signals. This framework includes three modules: (1) Static Multipath Removal: make a difference between CSI readings from different time instances to eliminate the effects of static multipath, (2) Interfering Dynamic Multipath Cancellation: utilize metrics for identifying signals in the frequency and spatial domain in which interfering dynamic multipath is canceled, and (3) Noise Reduction for Accurate Phase Difference Extraction: exploit the time diversity to suppress the impact of noise and extract the phase difference for ToF estimation.
4) We build a prototype using commodity WiFi devices. Extensive experimental results demonstrate that the system's performance in various scenarios with different noise, static multipath, and dynamic multipath conditions all outperform the state of the art [9]. SigCan can achieve a mean estimation error of 15.36 cm for humans in outdoor scenarios. More than 93% of the tested positions can be estimated reliably with a mean estimation error of 21.05 cm in different complex indoor environments for humans.

II. Related Work

ToF estimation for a target relies on the time delay [13] or the phase difference [14] introduced by the target path. Time delay can be calculated using Round Trip Time (RTT), which is further defined as a Fine Timing Measurement (FTM) in the IEEE 802.11-2016 standard [15]. However, such a method requires high hardware demands and calibration [3] for accurate time delay detection. MFDL [14] explore the phase delay among subcarriers for estimating distance and performs well in the outdoor environment. However, in practical indoor scenarios, signals reach the receiver through numerous propagation paths, leading to the phase difference or time delay induced by the target path being easily obscured by the impacts of multipath. To disentangle the parameters of the target path from the influence of multipath, previous methodologies can be typically categorized into two groups: approaches focused on enlarging bandwidth and techniques utilizing multidimensional information.

The first category of approaches focuses on improving range resolution by enlarging bandwidth. A few papers on WiFi-based localization leverage channel hopping such as ToneTrack [16], [17] to increase the bandwidth used for ToF estimation. ToneTrack measures differences in the ToF but cannot measure the absolute ToF. ToneTrack also requires the deployment of multiple APs in the environment. Chronos [7] and Splicer [13] leverage the CSI information across subcarriers to estimate the ToF of the direct path for trilateration-based localization. These methods necessitate measurements for calibration across multiple channels, thereby imposing constraints on real-world applications. These methods achieved better accuracy by combining channels to create a virtual wider bandwidth, enabling finer resolution. However, the channel hopping integral to these systems does impact data communication, which also limits their application.

The second category of methods seeks to enhance multipath resolution by leveraging information from multiple dimensions, such as ToF, AoA, DFS, and AoD. In scenarios where bandwidth limitations result in low ToF resolution, these paths may be differentiated through the AoA dimension. For example, SpotFi [18] and WiDeo [19] jointly estimate AoA and ToF for higher resolution. However, these two dimensions limit the upper bound of resolution. Besides, they face the challenge of high computational complexity, making it hard to be extended to more dimensions. Both mD-Track [8] and Widar2.0 [9] employ these four parameter dimensions to improve multipath resolution. mD-Track also reduces the computational complexity by proposing a linear-time estimator with a coordinate descent method. NLoc [20] also extracts multi-dimensional parameters for localization under Non-Line-of-Sight. However, these works rely on the collection of multidimensional information, imposing fresh requisites on both the hardware and software of WiFi devices. For instance, obtaining the AoA and AoD mandates prior knowledge of antenna positions within an array, ideally spaced at intervals near half a wavelength. However, antennas in commercial WiFi devices are primarily designed for communication, allowing for movable positions and existing across various polarization planes. These designs fail to meet the criteria for acquiring AoA, thus presenting challenges in implementing these methods to distinguish multipath on commercial WiFi devices.

Previous works have been predominantly focused on distinguishing the parameter information of multipath to extract the phase difference or time delay introduced by the target path. Additionally, these studies have commonly regarded increasing bandwidth as a necessary condition to enhance multipath resolution in a single ToF dimension. Otherwise, seeking information from alternative dimensions becomes the only way to differentiate multipath effects. However, this paper aims to propose a new way towards reliable ToF estimation on commodity WiFi devices. In typical daily single-person scenarios, it is disclosed that the signal cancellation between different interfering multipaths could make the phase difference introduced by the target path immune to multipath effect, thereby achieving accurate ToF estimation even with limited bandwidth.

III. Understanding ToF Estimation with WiFi Signals

In this section, we start by describing the basis of ToF estimation using phase differences of signals on multiple WiFi subcarriers in an ideal scenario (Section III-A). Then, we will model the signals that can be obtained from existing WiFi devices in real-world environments and analyze the phase differences across multiple subcarriers in Section III-B. We ultimately elucidate the challenges posed by real-world scenarios to ToF measurement using the multi-subcarrier phase difference method in Section III-C.

A. Modeling ToF Estimation Using Phase Differences in a Single-Path Scenario

We start by describing how CSI signals can be used for ToF estimation [21]. When the WiFi signal of frequency f traverses a path of length $d(t)$ from the transmitter (Tx) to the receiver (Rx) at time t, it introduces a delay, denoted as τ (i.e., ToF). This delay can be calculated as $\tau = \frac{d(t)}{c}$, where c represents the speed of light. Under an ideal condition (Rx can obtain accurate channel measurements without measurement noise), the wireless channel, influenced by this propagation path, yields the following measurement:

$$H(f,t) = \rho e^{-j2\pi f\tau} = \rho e^{-j\frac{2\pi d(t)f}{c}} \tag{1}$$

where ρ is the amplitude attenuation. This equation indicates that, for a given frequency f, as the length of the propagation path $d(t)$ increases, the phase change $\theta = \frac{2\pi d(t)f}{c}$ introduced by that path becomes more significant [22]. Conversely, if we were able to acquire the phase change $\frac{2\pi d(t)f}{c}$ that occurs during signal propagation, it becomes feasible to determine both the path length $d(t)$ and the ToF τ. Specifically, when there is only one propagation path in the environment, the phase of the channel measurement is solely a result of the phase change introduced by that propagation path.

However, the phase change obtained cannot be directly employed for ToF estimation due to the problem of phase wrapping,

which can be represented as follows:

$$\theta(f) = \frac{2\pi d(t) f}{c} \mod 2\pi \tag{2}$$

This phenomenon results in the phase change extracted from the signal losing cycle information, rendering the signal phase and the reflection path length not having a one-to-one correspondence. More specifically, when the phase change falls within the interval $[0, 2\pi]$, we can precisely measure ToF using the formula $\tau = \frac{\theta(f)}{2\pi f}$. However, if the phase change exceeds 2π, it wraps around and restarts from the opposite extreme, resulting in a phase change within the modulo 2π range. To put it differently, for a WiFi frequency of 2.4G Hz, propagation path lengths at distances separated by multiples of 12 cm (e.g., 3 cm, 15 cm, 27 cm, 39 cm, etc.) all yield the same channel phase change, i.e., $\pi/2$. Consequently, it becomes impossible to differentiate between these lengths with a single frequency based on the phase change information. In real-world scenarios, the length of signal propagation paths often extends to several meters or even tens of meters. Consequently, utilizing phase changes of a single subcarrier to measure the reflection path length (i.e., ToF) in real-world scenarios clearly encounters significant distance ambiguity.

To ensure an unambiguous estimation of propagation path length even when the path length is large, one approach is to reduce the signal's frequency. Drawing from fundamental principles of electromagnetics, it is well-established that as a signal propagates over time, it accumulates a phase change that is contingent upon its frequency. Signals with lower frequencies amass phase changes at a slower rate.

However, under the 802.11 protocol, the frequencies of WiFi subcarriers are fixed, and we cannot directly obtain a lower-frequency signal from existing devices. Therefore, we explore the possibility of utilizing existing subcarriers to construct a virtual signal with a lower frequency. Within the field of WiFi communication, we observe that the frequency interval between adjacent subcarriers (denoted as f_1 and f_2) in a 20 MHz bandwidth amounts to 312.5 kHz. Inspired by the facts, we create a virtual "subcarrier" by taking the difference between two subcarriers within the channel that have a small frequency interval, denoted as $\Delta f = f_2 - f_1$. Following propagation along the same path as the original subcarrier, the phase change of this virtual "subcarrier" $\theta(\Delta f)$ is equal to the phase difference between subcarriers f_2 and f_1, which can be written as follows:

$$\theta(\Delta f) = \theta(f_2) - \theta(f_1) = \frac{2\pi d f_2}{c} - \frac{2\pi d f_1}{c} = \frac{2\pi d \Delta f}{c} \tag{3}$$

When this virtual signal propagates along a given path to the receiver, its lower frequency prevents phase wrapping, thereby eliminating ambiguity in distance estimation. Taking the WiFi protocol as an example, the adjacent subcarrier frequency interval is 312.5 kHz. When the path length reaches 960 meters, the phase change corresponds to 2π, meaning that within 960 meters, any position has a unique phase value associated with it, eliminating ambiguity. This is sufficient to meet the requirements of most everyday applications. Therefore, we use the phase difference calculated by two subcarriers to estimate the propagation path length (i.e., ToF).

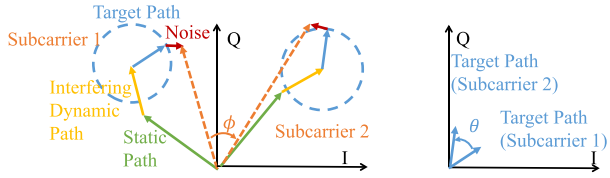

Fig. 2. Multipath components and ambient noise hinder us from extracting the phase difference introduced by the target path. We take CSI readings from two different subcarriers as an example to demonstrate that the phase difference ϕ affected by the multipath and noise is no longer equal to the phase difference θ introduced by the target path.

In summary, considering only one propagation path and no noise, we can directly calculate the phase difference $\theta(\Delta f)$ through channel measurements of different subcarriers. Subsequently, we can estimate the ToF for this path using the formula $\tau = \frac{\theta(\Delta f)}{2\pi \Delta f}$, given the value of Δf.

Takeaway: In a noise-free, single-path scenario, ToF measurements require only the phase difference collected from two subcarriers with a small frequency interval, such as a narrow bandwidth.

B. Phase Differences in Real-World Scenarios

Obtaining the ToF of the signal reflected by a person's body can enable various intelligent applications. However, in reality, acquiring the ToF of this path based on multi-subcarrier phase differences is not as straightforward as in ideal scenarios. First, ambient noise is inevitable in channel measurements. Second, in real-world environments, signals usually traverse multiple paths before reaching the receiver, introducing variations in channel measurement. Therefore, channel measurement, often referred to as CSI, acquired from transceivers, is a superposition of signals propagated through multiple paths. CSI can be modeled as follows [23]:

$$\begin{aligned} H(f,t) &= \sum_{l=1}^{L} \rho_l(f,t) e^{-j2\pi\tau_l f} + \epsilon(f,t) \\ &= \underbrace{\rho(f,t) e^{-j2\pi f \frac{d(t)}{c}}}_{①} + \underbrace{\sum\nolimits_{s=1}^{S} \rho_s(f) e^{-j2\pi f \frac{d_s}{c}}}_{②} \\ &\quad + \underbrace{\sum\nolimits_{m=1}^{M} \rho_m(f,t) e^{-j2\pi f \frac{d_m(t)}{c}}}_{③} + \underbrace{\epsilon(f,t)}_{④} \end{aligned} \tag{4}$$

where L denotes the total number of propagation paths, with l as the index of each path. S denotes the number of static propagation paths, with s as the index of each static path. M represents the number of interfering dynamic paths, with m as the index for interfering dynamic paths. $\epsilon(f,t)$ accounts for ambient noise (④), which adheres to a Gaussian distribution [12] (Red vector in Fig. 2).

Target path (①) refers to the propagation path that reaches the receiver only after a single reflection off the human target.

Its representation in the complex plane is a time-varying vector, with the phase changing as the person moves. To estimate the ToF of the target path, we need to extract the phase difference introduced by the target path on different subcarriers (Blue vector in Fig. 2).

Static multipath (②) refers to propagation paths whose lengths remain constant over time, such as the direct path or reflection paths via static objects in the environment. Their impact on the signal is represented as a vector with constant amplitude and phase that do not vary over time (Green vector in Fig. 2).

Interfering Dynamic multipath (③) refers to the propagation path that reaches the receiver after multiple reflections off the human target and the surrounding environment. With the movement of the human target, the path lengths of interfering dynamic multipaths change, leading to variations in phase. It also appears as a time-varying vector in the complex plane (Yellow vector in Fig. 2).

The phase of the signal at a given frequency results from the combined effects of the target path component, static multipath components, interfering dynamic components, and ambient noise, as shown in Fig. 2. As a consequence, the phase differences $\theta(\Delta f)$ calculated via the signal on different subcarriers no longer provide a direct indication of the ToF information related to the target. Hence, we need to extract the phase difference introduced by the target path across different subcarriers from the superimposed signals in order to estimate the ToF of the target path.

C. Extracting Phase Difference From Superimposed Signal

To extract the desired phase difference from superimposed signal, we need to eliminate the influence of other multipaths on the phase and reduce the impact of noise on the phase.

1) Multiple Path: Extracting ToF of the target path from signals superimposed with multiple paths (i.e., phase difference between subcarriers for our work, signal delay for previous work) is a common challenge in related research [24]. Previous studies have shown that time delay resolution $\Delta\tau$ is correlated with bandwidth. Specifically, as the bandwidth increases, the time delay resolution also improves, and this relationship can be expressed as $\Delta\tau = \frac{1}{B}$, in which B is the bandwidth used for ToF estimation.

With a sufficiently large bandwidth, even paths with small differences in ToF can be distinguished. The assistance of a large bandwidth allows the separation of mixed superimposed signals into individual signal propagation paths. At this point, the signal variations introduced by the target path can be clearly extracted.

However, due to protocol limitations, WiFi signals cannot access sufficiently large bandwidths. If we aim to achieve ToF estimation for a single target in indoor environments within a single WiFi channel, we must ensure that the signal can be treated as if it contains only the target path, preventing the influence of static multipath and interfering dynamic multipath on the phase differences.

2) Ambient Noise: Ambient noise in the signal also pollutes the phase difference across different subcarriers introduced by the target path. As shown in Fig. 2, the ambient noise will introduce a large extra phase difference between signals in different subcarriers.

While earlier research has made efforts to segregate the multipath, they often give limited consideration to the impact of ambient noise. Prior approaches either rely on single data packets for ToF estimation (as exemplified by methods like mD-Track [8]) or simply average the results obtained from multiple data packets [20].

When the strength of noise is low, the phase differences introduced by noise are distributed within a small range, and the mean converges to the true value [25]. With a large number of samples, the impact of noise can be reduced, allowing for the estimation of the true phase difference. However, when noise intensity is high, we can prove that the mean of signal samples no longer converges to the actual phase difference. Moreover, the mean of phase difference changes as noise increases. In such situations, directly averaging multiple independent estimates does not improve the precision of phase difference estimation. This necessitates the development of new methods that can accurately extract phase differences even in situations with higher noise levels.

IV. Overview of SigCan ToF Estimation Framework

In this section, we provide an overview of SigCan ToF estimation framework. The key idea for the target path ToF estimation in the complex multipath environment is preventing the phase difference from being polluted by static multipath, interfering dynamic multipath, and noise through signal cancellation. Due to the distinct properties of static multipath, interfering dynamic multipath, and noise, we suggest employing specific elimination methods tailored to the characteristics of different signal components as shown in Fig. 3:

1) Static Multipath Removal: Our observations reveal that the static environment experiences minimal change over short time intervals, resulting in a constant impact on the signal. Thus, we eliminate the static multipath component by taking a difference between CSI readings obtained at distinct time instances in one subcarrier. We present the detailed static multipath elimination method in Section V.

2) Interfering Dynamic Multipath Cancellation: We observed that when signals with a given wavelength propagate along two paths whose path lengths differ by half a wavelength, the signal variations introduced by the two paths cancel each other out, rendering both paths no longer impactful on the signal's phase. With abundant superposition from frequency and spatial diversity, we envision such conditions can be found. We propose utilizing the signal where interfering dynamic multipath components mutually cancel each other out for ToF estimation, thereby diminishing the impact of dynamic multipath interference.

However, even if there exists a signal with dynamic multipath cancellation, there is no straightforward way to find this signal from a variety of candidate signals. To address this, we design

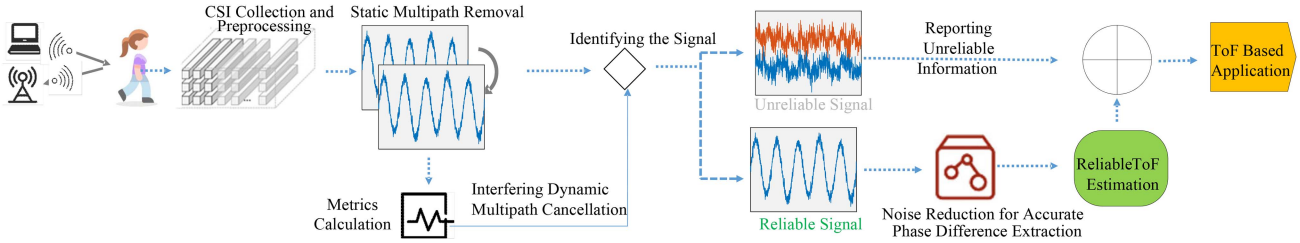

Fig. 3. Overview of the Framework.

metrics to help us determine which signals experience multipath cancellation. We present our metrics in Section VI.

3) Reducing the Influence of Noise for Accurate Phase Difference Extraction: To obtain an accurate phase difference, mitigating the impact of ambient noise is crucial. Ambient noise, following an independent Gaussian distribution in the complex plane [12], [26], [27], tends to mutually cancel out with a large number of samples, as supported by the Kolmogorovâs Strong Law of Large Numbers. Hence, we propose an algorithm that utilizes multiple samples in the complex plane to diminish the influence of noise on phase difference extraction. We present our algorithm in detail in Section VII.

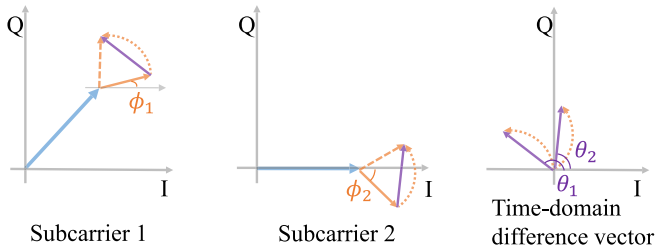

Fig. 4. Schematic for eliminating static multipath components. We leverage the CSI readings in different time instances to cancel the static multipath components during which the static component stays constant.

V. Static Multipath Removal

We remove the static multipath component via CSI readings collected at different time instances, ensuring that the phase difference remains uncontaminated by static multipath component. We will first outline the process in Section V-A and subsequently verify the feasibility of the method in Section V-B.

A. Utilizing Multiple Time-Domain CSI Readings for Static Multipath Removal

We discuss the following two aspects: (1) modeling the process of eliminating static components via CSI samples from different time instances in one subcarrier, and (2) extracting the phase difference caused by the target path from the signal after static multipaths cancellation.

Modeling the process of eliminating static components: To focus on the discussion of static multipaths, we first simplify the scenario by assuming there is no interfering dynamic multipath or noise. In this case, CSI is only affected by the static multipath and the target path, which can be represented as follows:

$$H(f,t) = \sum_{l=1}^{L} \rho_l(f) e^{-j2\pi f \frac{d_l}{c}} + \rho(f,t) e^{-j2\pi f \frac{d(t)}{c}} \quad (5)$$

We then eliminate the static multipath component by taking a difference between CSI readings obtained at distinct time instances (t and t_0) in one subcarrier. We observe that the dynamic vector introduced by the target path changes over time (Orange vector in Fig. 4), while the static vectors introduced by static multipath (Blue vector in Fig. 4) remain constant over time. Consequently, after computing the differences in CSI readings collected from one subcarrier, the static multipath components are eliminated. The target dynamic vector is transformed into a new vector, referred to as the time-domain difference vector (Purple vector in Fig. 4). The process is presented as follows:

$$\begin{aligned} E(f,t) &= H(f,t) - H(f,t_0) \\ &= \rho(f,t) e^{-j2\pi f \frac{d(t)}{c}} - \rho(f,t_0) e^{-j2\pi f \frac{d(t_0)}{c}} \end{aligned} \quad (6)$$

According to the formula, the time-domain difference vector is determined by the target path, indicating that the static multipath component has no impact on the new signal.

It's important to emphasize that there is no specific requirement for the time interval between t and t_0 as long as the static components remain constant. This requirement can be easily satisfied when the sampling interval is short enough (i.e., the sampling rate is high). When the target moves within a small range, the sampling rate can be low.

Extracting the phase difference from time-domain difference vector: However, there occurs a new question, i.e., whether the phase difference of the time-domain difference vector across different subcarriers can still be used for the target's ToF calculation (i.e., whether $\theta_2 - \theta_1$ is equal to $\phi_2 - \phi_1$ as shown in Fig. 4).

To answer the question, we first divide the path length into two parts, namely, $d(t) = d(t_0) + \Delta d(t)$. In this equation, $d(t_0)$ signifies the path length at time t_0, while $\Delta d(t)$ represents the variation in path length at time t compared to that at time t_0. This formulation can be written as follows:

$$\begin{aligned} E(f,t) &= H(f,t) - H(f,t_0) \\ &= e^{-j2\pi f \frac{d(t_0)}{c}} \rho(f,t) \left(e^{-j2\pi f \frac{\Delta d(t)}{c}} - 1 \right) \end{aligned} \quad (7)$$

According to the formula, the phase comprises two components: $2\pi f \frac{d(t_0)}{c}$, which is determined by the target path length

at time t_0, and $Arg(e^{-j2\pi f\frac{\Delta d(t)}{c}}-1)$ which is associated to the movement. Given that the value of $d(t_0)$ may range from several meters to tens of meters, $2\pi f\frac{d(t_0)}{c}$ induces substantial phase differences across various subcarriers. Consequently, we can calculate the ToF of the target at time t_0 based on this term. When the target moves within a small range, such as waving a hand or breathing, signal phase $Arg(e^{-j2\pi f\frac{\Delta d(t)}{c}}-1)$ caused by the minor movement $\Delta d(t)$ among different subcarriers is nearly the same. For instance, when the target path length varies over time within 10 cm, the maximum phase changes for the two subcarriers at 5.3 GHz and 5.32 GHz are 11.1003 radians and 11.1422 radians, respectively. If we disregard the phase difference, it would lead to a maximum error of approximately 0.33 ns in ToF or 10 cm in path length. Since there are multiple samples collected during the movement, the average error is 5 cm in path length. Moreover, if the subject performs periodic movements within a small range, such as breathing, where the target path length oscillates around the path length at time t_0, then the average error will approach 0. The analysis indicates that smaller movement amplitudes of the target result in lower impact from assuming the phase difference of $Arg(e^{-j2\pi f\frac{\Delta d(t)}{c}}-1)$ is consistent across different subcarriers, leading to more accurate estimates. When estimating ToF during slight body movements or breathing, the theoretical error is only a few millimeters or centimeters.

Therefore, the phase difference among time-domain difference vectors from different subcarriers is dominated by the target path and can be rewritten as follows:

$$\angle E(f_2,t)-\angle E(f_1,t)=2\pi\Delta f\frac{d(t_0)}{c} \tag{8}$$

The formula affirms that the phase difference among time-domain difference vectors from different subcarriers can be used to estimate the target's ToF without introducing bias.

B. Verification of Static Multipath Component Elimination

We experimented under the condition featuring one dynamic path (i.e., the target path) and multiple static paths without noise, to verify (1) the effectiveness of static multipath elimination methods and (2) the capability to measure the ToF of the target path using a narrow bandwidth, where only the target path remains after static multipath cancellation.

Experimental Setup: In an open outdoor environment, we positioned a pair of WiFi transceivers and a metal plate (measuring 30 cm in height and 20 cm in width) as shown in Fig. 5(a). The distance between transceivers was 1 m. The metal plate, acting as an ideal reflector for radio waves, was moved within 3 cm along an electric control slide rail. We systematically displaced the metal plate at different positions along the perpendicular bisector to the Line of Sight (LoS). The distance between the plate and the transceivers ranged from 2 meters to 6 meters. We employed the method described above to calculate the phase difference for ToF estimation. In such an outdoor environment, the conditions can be met: (1) The static conditions remain constant and stable, and (2) There exists only one dynamic path (i.e., reflection off plate). Despite the presence of noise in the CSI readings, we have maintained a relatively high signal-to-noise ratio through time diversity [12].

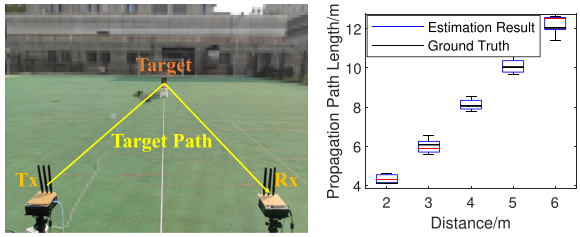

(a) Experimental Setup (b) ToF Estimation Result

Fig. 5. Empirical study in an outdoor scenario to verify the static multipath elimination. The result shows that we can use the method to accurately estimate the ToF using 4 CSI readings from 2 subcarriers in a scenario with a single target path and multiple static paths.

Experiment Result: Fig. 5(b) displays the estimated path length (i.e., ToF multiplied by the speed of light) calculated using four samples from subcarrier 11 and 16 provided by CSI tool [28] for various positions of the plate. The frequency interval between subcarrier 11 and 16 is approximately 4 MHz. The average error between the estimated path length and the ground truth is approximately 32.55 cm. This result demonstrates the static multipath component is successfully eliminated, enabling accurate measurement of the target path ToF using a narrow bandwidth, where only the target path remains after static multipath cancellation.

VI. Interfering Dynamic Multipath Cancellation

By leveraging the interfering dynamic multipath cancellation, we have the opportunity to extract phase differences unaffected by interfering dynamic multipath in real-world scenarios, enabling the estimation of the target path's ToF (Section VI-A). However, the challenge lies in identifying signals that undergo interfering dynamic multipath cancellation from the received multitude of signals. Therefore, we propose two metrics for quantifying the cancellation among interfering dynamic multipath in Section VI-B. We validate the effectiveness of these metrics through experiments in Section VI-C.

A. Leveraging Signal With Interfering Dynamic Multipath Cancellation for ToF Estimation

After being processed by the method in Section V, the input signal can be written as follows:

$$\begin{aligned}E(f,t)&=H(f,t)-H(f,t_0)\\&=e^{-j2\pi f\frac{d(t_0)}{c}}\rho(f,t)\left(e^{-j2\pi f\frac{\Delta d(t)}{c}}-1\right)\\&\quad+\sum_{m=1}^{M}\rho_m(f,t)e^{-j2\pi f\frac{d_m(t)}{c}}-\sum_{m=1}^{M}\rho_m(f,t_0)e^{-j2\pi f\frac{d_m(t_0)}{c}}\\&\quad+\epsilon(f,t)-\epsilon(f,t_0)\end{aligned} \tag{9}$$

If we can identify the signal in which the dynamic multipath cancel each other out and introduce weak or negligible influence

to the phase difference, we can transform (9) to (7) with noise, which allows us to calculate the ToF of the target path using a narrow bandwidth.

We start by explaining why we believe there exists such kind of signal where the interfering dynamic multipath components cancel each other out. For a given subcarrier with wavelength λ, the propagation path at time t with length $d_1(t)$ will introduce a phase change of $\frac{2\pi d_1(t)}{\lambda}$. Given the numerous propagation paths in the environment, there may be another path at time t with length $d_2(t) = d_1(t) + \frac{\lambda}{2} + \lambda \cdot k, k \in [0, \pm 1, \pm 2, \dots]$, introducing a phase change of $\frac{2\pi d_2(t)}{\lambda} = \frac{2\pi d_1(t)}{\lambda} + (2k+1)\pi, k \in [0, \pm 1, \pm 2, \dots]$. The second phase change is opposite to the phase change introduced by the first path. When WiFi signal arrives at the receiver along these two paths, their influences at time t will cancel each other out, ensuring they do not affect the phase.

With abundant samples from spatial diversity (samples collected in different antennas) and frequency diversity (samples collected in different subcarriers), it's highly possible to find a signal in which dynamic multipath components introduce weak or even no influence on the phase. The positional differences among antennas result in signals arriving at different antennas with varying propagation path lengths, thereby introducing different phases across antennas. This variability in superposition among antennas also applies to frequency diversity, where signals arriving at the same antenna but on different subcarriers introduce different phases. This diversity in signal superposition across subcarriers increases the likelihood of identifying signals where dynamic multipath cancel each other out.

Specifically, when the target moves within a small range, such as breathing, the path lengths also change over time due to target movement. However, the interfering dynamic multipath components may still cancel out at different times because the superpositions approximately remain constant due to the minimal path length changes.

B. Metrics for Identifying Dynamic Multipath Cancellation

To identify the signal undergoing interfering dynamic multipath cancellation from abundant signal samples, we propose two metrics as indicators, which were inspired by the following observations.

Observation from a Single Time Instance: In situations where static multipath and interfering dynamic multipath components were canceled and the target path with length d dominates the signal variation, the phase of the signal collected on subcarrier f can be expressed as $\theta = -\frac{2\pi df}{c}$. The phase of different subcarriers after phase unwraping decreases linearly due to the increasing frequency f. In other words, the phase at a given time across different subcarriers exhibits a linear relationship when there is only one target path in the environment.

When multiple propagation paths affect the phase, the phase across multiple subcarriers may no longer exhibit a linear relationship. Therefore, we propose a metric to evaluate the linearity of phase difference across multiple subcarriers, which further helps identify the signal undergoing multipath cancellation.

Observation from Multiple Time Instances: The signal pattern over time in the complex plane is determined by the amplitude and phase. If the multipath component is canceled, the signal pattern is dominated by amplitude and phase related to the target path. When the path length change is within a small range, i.e., the target moves within a small range, the phase change during the movement among different subcarriers will be nearly identical and the amplitude also remains constant. Consequently, the signal pattern among different subcarriers will be nearly identical.

When multiple propagation paths superimpose and contribute to the signal pattern simultaneously, the phase and amplitude will change due to variations in any one of the propagation paths. This results in the signal patterns collected across multiple subcarriers at distinct time instances being distorted due to the different superpositions. We propose another metric to measure the similarity of signal patterns across multiple subcarriers. Higher similarity indicates a weaker multipath component, making it more suitable for ToF estimation.

Based on the insight above, we propose two metrics to identify signals undergoing interfering dynamic multipath cancellation.

Metric 1: We propose the first metric to evaluate the linear relationship among the phases of different subcarriers.

Definition of Metric 1: In statistics, the correlation coefficient is used to quantify the linear relationship between two random variables. When we apply the correlation coefficient for evaluating the linear relationship among phases, it can be calculated using the following formula:

$$R(\Delta f, \Delta\theta(\Delta f)) = \frac{cov(\Delta f, \Delta\theta(\Delta f))}{\sigma_{\Delta f} \cdot \sigma_{\Delta\theta(\Delta f)}} \tag{10}$$

We marked $R(\Delta f, \Delta\theta(\Delta f))$ as Metric 1. In this equation, Δf represents the frequency interval between different subcarriers. For example, since we can collect signals from 30 different subcarriers with CSI tool [28], the frequency interval between subcarriers 2–29 and subcarrier 1 is denoted as Δf, and its range is [625 kHz, 20 MHz]. $\sigma_{\Delta f}$ means the standard deviation of Δf. $\Delta\theta(\Delta f)$ represents the phase difference of the time-domain difference vector. $cov(\Delta f, \Delta\theta(\Delta f))$ indicates the covariance of Δf and $\Delta\theta(\Delta f)$.

If a subset of signals from different subcarriers undergoes dynamic multipath cancellation, the value of the metric will approach 1. Therefore, we will consider using this subset of signals as input.

Metric 2: We propose the second metric to evaluate the similarity of signal patterns across different subcarriers on the complex plane.

Definition of Metric 2: We assess similarity by measuring the distances between corresponding sampling points from different subcarriers on the complex plane. We observed that when two signals exhibit identical patterns, their samples in the complex plane overlap at any given time, resulting in a total distance of 0 at multiple time instances. However, the varying interfering dynamic multipath components in different subcarriers introduce different signal variations and distort the signal pattern introduced by the target path, leading to larger distances between corresponding sampling points. Therefore, we utilize distance as the second metric. It should be noted that even if the signal undergoes dynamic multipath cancellation as shown in (7), there may still be a significant distance between subcarriers due to the

Algorithm 1: Identifying the Signal Undergoing Interfering Dynamic Multipath Cancellation.

Input: Time-domain difference vector $E(f,t)$
Output: Reliable Flag & Subcarriers used for ToF Estimation
foreach antennas **do**
  Selecting one subcarrier r as the reference;
  foreach subcarriers i **do**
    Calculating $\Delta\theta(\Delta f_{r,i})$;
    Calculating $D(f_r, f_i)$;
  end
  Searching for a consecutive set of $N(>20)$ subcarriers $[f_j, f_{j+N}]$ where Metric 1 and Metric 2 exceeds the predefined threshold.;
  if empty **then**
    Reliable Flag=0;
  else
    Reliable Flag=1;
    Output $[f_j, f_{j+N}]$;
  end
end

different initial phases (i.e., $2\pi f \frac{d(t_0)}{c}$). Therefore, we adjust the phase and position of the signal and then utilize the minimum distance between subcarriers to represent the similarity.

$$D(f_1, f_2) = \min \frac{1}{T} \sum_{t=1}^{T} |H(f_1, t) - \hat{H}(f_2, t)| \qquad (11)$$

where $H(f_1, t)$ indicates the CSI from subcarrier f_1 and $\hat{H}(f_2, t)$ indicates the adjusted CSI from subcarrier f_2. If a subset of signals from different subcarriers undergoes dynamic multipath cancellation, the value of the second metric between any two of the subcarriers will approach 0. Therefore, we will consider using this subset of signals as input.

Leveraging the metrics for signal selection: We utilize the metrics to select a subset of signals from frequency diversity and spatial diversity where the interfering dynamic multipath components cancel each other out, thereby providing a reliable and accurate ToF estimation of the target.

Specifically, for each antenna, we select contiguous k subcarriers where the value of the metrics meets the predefined threshold. Once k surpasses another specified threshold (where a larger k implies higher estimation precision but presents greater difficulty in satisfying), it is recognized as a candidate set. The candidate set with metric values closest to the ideal condition is then chosen for ToF estimation.

However, in complex scenarios where canceling interfering dynamic multipath is challenging, particularly in proximity to strong reflectors, our methods cannot consistently find the CSI under the ideal condition. In these instances, we can choose comparatively better signals from the set, resulting in an unreliable estimation of the current position. We present the process as shown in Algorithm 1.

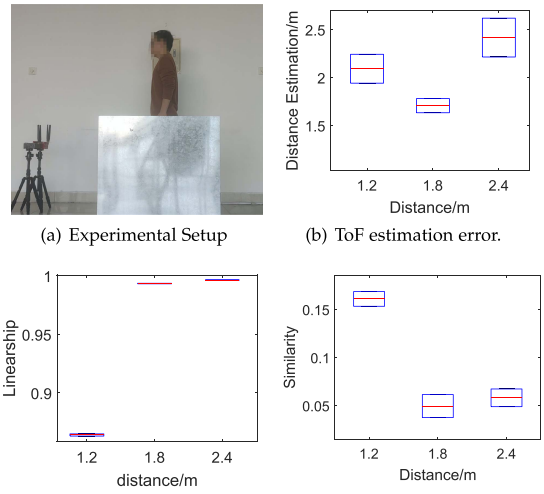

(a) Experimental Setup (b) ToF estimation error.
(c) Linear relationship(metric 1). (d) Similarity (metric 2).

Fig. 6. Empirical study in a multipath scenario. The result shows that the metric can identify the signal in which the dynamic multipath components cancel each other so that the ToF estimation result is accurate.

C. Verification of Metrics Validity

To validate the effectiveness of these metrics for identifying the signal with multipath cancellation, we conducted a series of experiments. The validation process consists of two parts:

1. When the impact of interfering dynamic multipath components is negligible, the metrics should indicate well (high similarity and good linear relationship). The ToF estimation shall be accurate with these signals.
2. When the impact of interfering dynamic multipath component is significant, the metrics should deteriorate (similarity decreases, linear relationship worsens). The ToF estimation shall be inaccurate with these signals.

Experimental Setting: We conducted experiments in an empty laboratory. We positioned the subject at various locations and instructed them to shake their body. To create strong dynamic multipath, we placed a large metal plate as a reflector 1.2 meters away from the device. When the subject stood near the large metal plate, as shown in Fig. 6(a), signals were reflected from the subject and the metal plate, introducing a strong interfering dynamic multipath. When the subject stood farther away from the large metal plate, the interfering dynamic multipath components were weaker. We calculated the metrics when the subject stood at different positions. We also applied the method described in Section V to calculate the ToF to verify if the ToF is accurate when the metrics indicate the signal undergoes interfering dynamic multipath cancellation.

Experiment Result: As shown in Fig. 6, when the subject stands far away from the large metal plate, such as at 1.8 m and 2.4 m, the interfering dynamic multipath component is negligible. The phase across the subcarriers maintains a linear relationship (metric 1 is larger than 0.99), and the corresponding signal samples are close in the complex plane (metric 2 is below 0.07). The phase difference caused by the subject approaches the theoretical value, resulting in a mean estimation error of 11.73 cm in distance estimation.

When the subject stands near the large metal plate (1.2 meters from the devices), the phase across the subcarriers does not exhibit a significant linear relationship (metric 1 is lower than 0.87) and the corresponding signal samples are far apart due to the interfering dynamic multipath. The mean distance between samples from different subcarriers is around 0.16 in the complex plane, which is much larger than the distance when the subject stands far away from the reflector.

By leveraging the metrics, we can identify the signal undergoing interfering dynamic multipath cancellation for accurate ToF estimation.

VII. Noise Reduction for Accurate Phase Difference Extraction

CSI contains various types of noise that affect the phase difference. While some of the noise has been addressed as described in Section VII-A, ambient noise still impacts the phase differences across different subcarriers, introducing errors in ToF estimation. In this section, we focus on extracting accurate phase differences in the presence of ambient noise. We propose to leverage multiple samples in the complex plane to reduce the influence of noise in Section VII-B, followed by the method's verification in Section VII-C.

A. Noises in Real WiFi Signals and CSI Ratio

In reality, CSI readings collected from commodity WiFi devices contain severe noise comprising of the impulse noise in CSI amplitude [23], random offset in CSI phase [13], [18], [29], [30], which affects the phase difference. The CSI readings obtained from commodity WiFi devices are the composition of the ideal wireless channel and noise:

$$H(f,t) = A_{\text{noise}}(f,t)e^{-j\theta_{\text{offset}}(f,t)}H_{air}(f,t) + \epsilon(f,t) \quad (12)$$

where $\epsilon(f,t)$ indicates the ambient noise, $A_{\text{noise}}(f,t)$ is the impulse noise in amplitude, $\theta_{\text{offset}}(f,t)$ is the random phase offset, $H_{air}(f,t)$ is the ideal wireless channel state in the air.

Since it has been observed that time-varying CSI amplitude impulse noise and phase offset exhibit uniform characteristics across different antennas on a WiFi Network Interface Card, researchers have introduced a concept known as CSI Ratio [31], [32], [33]. This ratio is calculated as the quotient of CSI readings obtained from two antennas on the same WiFi receiver, and its purpose is to effectively eliminate both the CSI amplitude noise and phase offset [34], [35], [36], [37]. We demonstrate that the phase difference of the CSI Ratio across different subcarriers can still be used for ToF estimation. We can eliminate the distortion caused by denominator using a calibration-based method when the static component is larger than the dynamic component.

B. Leveraging Large Numer of Samples for Reducing Impact of Noise

After we process the input signal with the method in Section V and Section VI, the signal used in this section is the superposition of the time-domain difference vector and ambient noise, represented as follows:

$$E(f,t) = e^{-j2\pi f\frac{d(t_0)}{c}}\rho(f,t)\left(e^{-j2\pi f\frac{\Delta d(t)}{c}} - 1\right) + \epsilon(f,t) \quad (13)$$

Now, we focus on reducing the impact of noise to extract accurate phase differences of time-domain difference vectors among subcarriers.

Given a subcarrier with frequency f, $\epsilon(f,t)$ can be approximated as an additive white Gaussian noise with zero mean and a variance of $\sigma^2(f)$, *i.e.*, $\epsilon(f,t) \sim N(0,\sigma^2(f))$. The noises $\epsilon(f_1,t_1)$ and $\epsilon(f_2,t_2)$ are independent for any two different subcarriers $f_1 \neq f_2$ or any two different time slots $t_1 \neq t_2$ when the CSI is measured [12], [26], [27].

Inspired by the properties of noise, previous work usually estimates ToF with a single CSI sample [8] or packet [20] and then averages multiple ToF estimations to reduce the impact of noise. We envision that such a method will fail when the noise level is high. Ambient noise may introduce a large phase shift, causing the phase of the signal above to exceed π or $-\pi$, leading to phase wrapping. Consequently, the mean of these samples is not equal to the phase difference of the time-domain difference vector. As noise levels increase, more samples encounter phase wrapping, which hinders the mitigation of noise impact even with multiple samples.

To mitigate the influence of noise more effectively, we propose employing multiple samples concurrently. As demonstrated in Section V, the time-domain difference vectors of different subcarriers have identical signal patterns with different initial phases. The difference between initial phases is $2\pi\Delta f\frac{d(t_0)}{c}$, which can be used for ToF estimation. If we rotate the signals collected from different subcarriers by $2\pi\Delta f\frac{d(t_0)}{c}$, the samples collected at the same time from different subcarriers will overlap in the complex plane, i.e., the distance between corresponding samples will be zero when there is no noise in the signal. The distance between corresponding samples can be used to determine whether the phases of different subcarriers have been adjusted to the same and whether the rotation angle equals $2\pi\Delta f\frac{d(t_0)}{c}$.

Under noisy conditions, we can still utilize the distance between the corresponding samples from different subcarriers as an indicator to determine whether the rotation angle equals $2\pi\Delta f\frac{d(t_0)}{c}$, i.e., the phase difference introduced by the target's ToF. We formula the process as follows:

$$\begin{aligned}\arg\min_{\theta_{i,j}} Dis(f_i,f_j) &= \sum_{t=1}^{T}|E(f_i,t) - E(f_j,t)e^{j\theta_{i,j}}|^2 \\ &= \sum_{t=1}^{T}|\left(e^{-j2\pi f_i\frac{d(t_0)}{c}} - e^{j\theta_{i,j}}e^{-j2\pi f_j\frac{d(t_0)}{c}}\right) \\ &\rho(f_i,t)\left(e^{-j2\pi f_i\frac{\Delta d(t)}{c}} - 1\right) + \epsilon(f_i,t) - e^{j\theta_{i,j}}\epsilon(f_j,t)|^2 \quad (14)\end{aligned}$$

Given a sufficient number of samples, the distance related to the noise term $\epsilon(f_i,t) - e^{j\theta_{i,j}}\epsilon(f_j,t)$ remains nearly constant regardless of the rotation angle according to Kolmogorovâs Strong Law of Large Numbers. Due to space constraints, the complete proof process is not included here.

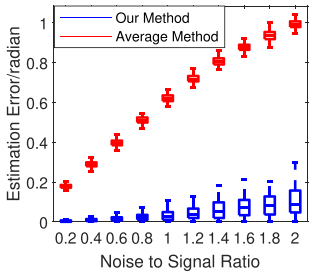

Fig. 7. Trace-driven experiment. As noise increases, our method can extract phase differences with limited error while previous work cannot.

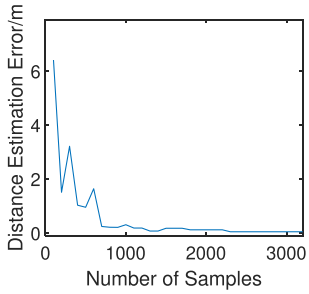

Fig. 8. More samples improved the accuracy of estimation.

Only when $\theta_{i,j}$ equals $\frac{2\pi d(t_0)\Delta f}{c}$ does the term $e^{-j2\pi f_i \frac{d(t_0)}{c}} - e^{j\theta_{i,j}} e^{-j2\pi f_j \frac{d(t_0)}{c}}$ reach its minimum value of 0, and the total distance also reaches its minimum value. We envision that by leveraging the distance between samples as an indicator, we can extract an accurate phase difference with sufficient samples.

C. Verification of Multiple Samples Based Phase Difference Extraction Method

1) Trace-Driven Emulation: We use a trace-driven emulation to assess the multiple samples based phase difference extraction method at different noise levels and compare it with the previous method that calculates the phase with a single sample and then averages the multiple phase difference estimations. Keeping other experimental setups the same as in Section V-B, we first collect a signal from a moving plate 2 m away from the transceivers. This signal is used as an approximation of a noise-free signal. The signal consists of 7800 samples with a sampling rate of 500 Hz. We then add different levels of Gaussian noise to this signal to emulate signals with various noise levels. Our emulated trace is fed into both methods (the averaging method and our proposed method) to extract the phase difference introduced by the target path.

We repeated the experiment 100 times under different noise levels and plotted the distribution of errors for the two methods under various noise levels using box plots in Fig. 7. The X-axis represents the noise-to-signal ratio while the Y-axis represents the mean absolute error. The result indicates that our method can still extract phase differences with limited error when the noise is larger than the signal.

2) Empirical Study: We now analyze the relationship between distance estimation error and the number of sampling points. Keeping other experimental setups the same as in Section V-B, we positioned the plate further from the devices (14 m–15 m) to obtain signals with a higher noise to signal ratio. We collected data for 16 seconds at a sampling rate of 500 Hz. We use the same dataset and obtain signals with different numbers of samples by discarding part of the samples (i.e., downsampling). The number of samples used for distance estimation ranged from 100 to 3200 in intervals of 100. As shown in Fig. 8, increasing the number of samples fed into the method improves the accuracy of the estimation. This demonstrates the crucial role that a sufficient number of samples plays in phase difference extraction. It should also be noted that with a lower noise-to-signal ratio, fewer samples are sufficient to meet the requirements for precise ToF estimation as have been demonstrated in Section V-B.

VIII. Evaluation

This section aims to evaluate the SigCan's capability in estimating ToF across diverse multipath conditions, focusing on two typical scenarios: (1) Indoor environments, where challenges arise from interfering dynamic multipath, static multipath, and noise; (2) Outdoor environments, primarily challenged by static multipath effects and ambient noise. Furthermore, we also assess the performance in daily life, showcasing SigCan's effectiveness in daily life.

A. System Implementation

1) Hardware: SigCan is built using commodity WiFi hardware, consisting of two WiFi devices: a WiFi transmitter (Tx) and a WiFi receiver (Rx), both equipped with Intel 5300 wireless cards. Each device has three external omnidirectional antennas. Unless explicitly stated otherwise, the system employs a 20 MHz bandwidth and a 500 Hz sampling rate. Additionally, a laptop with an Intel Xeon W-10855M CPU is used for data processing.

2) Software: SigCan consists of five modules: (1) Data Collection: With CSI tool [38], we collect CSI data from Intel 5300 wireless cards, which contain information from 30 subcarriers. Since the Intel 5300 wireless card supports three antennas, CSI data is a $3 \times 30 \times T$ complex matrix, where T represents the number of samples. This CSI data is sent to a laptop for further processing. (2) Data Pre-processing: we utilize CSI Ratio [34] to eliminate the phase offset of the data, resulting in a $3 \times 30 \times T$ complex matrix. (3) Static multipath removal: for each subcarrier (i.e., $1 \times 1 \times T$ matrix), we calculate the time-domain difference vector and obtain a new input signal, which is a $3 \times 30 \times (T-1)$ matrix. (4) Interfering Dynamic Multipath Identification: For each antenna, we first select one subcarrier as a reference. We then calculate metric 1 and metric 2 with other subcarriers and select the best-performing consecutive $N(>20)$ subcarriers on the two metrics as a candidate set. Finally, we choose the group with the best metric performance from the candidate sets on different antennas for estimation. (5) ToF Estimation Under Noisy Conditions: we utilize all the $T-1$ samples in the selected subset of subcarriers for ToF estimation, detailed in Section VII-B.

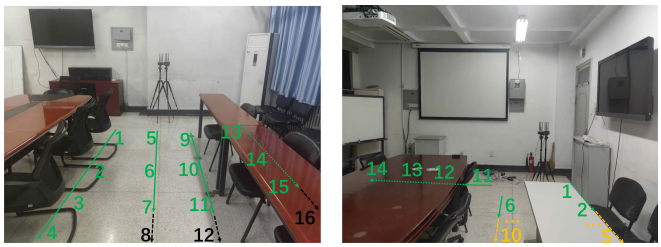

(a) Experiment setting of meeting room 1. (b) Experiment setting of meeting room 2.

Fig. 9. Experiment setting in two indoor environments.

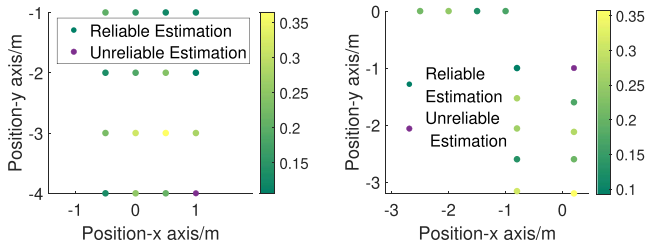

(a) Distance estimation error in meeting room 1. The unreliable estimated position corresponds to Position 16 in Fig.9(a). (b) Distance estimation error in meeting room 2. The unreliable estimated position corresponds to Position 1 in Fig.9(b).

Fig. 10. Distance estimation error in two indoor environments. Reliable estimation means we can utilize the metrics to find the signal with minimal interference of multipath for distance estimation while unreliable estimation means we cannot find such kind of signal.

B. Experimental Design

From the discussion above, we demonstrate the ability (1) to identify the signal undergoing interfering dynamic multipath cancellation and (2) to utilize such signals for ToF estimation after eliminating static multipath and reducing the influence of noise. Therefore, we evaluate the system from these two aspects, respectively.

We set up two different scenarios to evaluate the performance, respectively:

1) Indoor scenarios: we conducted the experiments in two meeting rooms as shown in Fig. 9(a) and (b). Here, we evaluate the metrics proposed in Section VI. First, we assess whether the estimated ToF is accurate for the locations where the metrics indicate favorable conditions. Second, we evaluate if the metrics can alert us when the interfering multipath is too strong to identify suitable signals for ToF estimation.

2) Outdoor scenarios: we selected a square as the experiment site as shown in Fig. 12, where there is nearly no interfering dynamic multipath. We aim to evaluate the robustness of the static multipath elimination method (detailed in Section V) and the noise influence reduction method (detailed in Section VII).

Additionally, we build a real-time distance estimation system and showcase its effectiveness in daily life scenarios, as shown in Fig. 19.

To comprehensively evaluate the system, we recruited 12 subjects and repeated the experiments multiple times on different days under various environments.

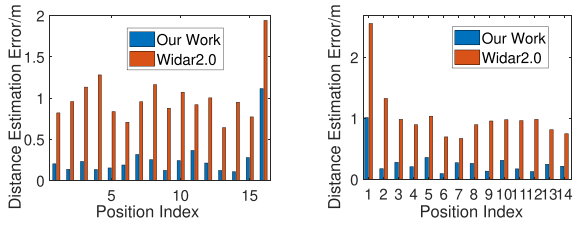

(a) Comparison with baseline in meeting room 1. (b) Comparison with baseline in meeting room 2.

Fig. 11. Distance estimation error in an indoor environment.

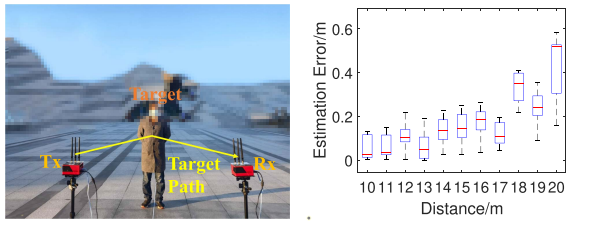

(a) Experiment setting. (b) Distance estimation error when sensing the human target 10m-20m away from devices.

Fig. 12. Distance estimation error in a outdoor environment.

1) Distance Estimation Error: We use the distance between the target and the device as a metric to evaluate the ToF estimation accuracy. When the target is equidistant to the transceivers (e.g., situated along the perpendicular bisector of the line connecting the Tx and Rx), or when the transceivers are in very close proximity to each other, we can estimate the distance between the target and the device by halving the reflection path length obtained from ToF. To obtain the actual distance, we utilize a laser rangefinder. We record the difference between the measured and estimated distances as the distance estimation error.

2) Baselines: Given that both mD-Track and Widar2.0 leverage multidimensional information for estimation, their performance should be similar. We compare the distance estimation accuracy with Widar2.0 [9], a system proposed for indoor localization. We replicated the work of Widar2.0 using their publicly available code to facilitate a comparative analysis. To ensure a fair comparison with Widar2.0, we replaced Widar2,0's input signal with CSI Ratio [34], maintaining consistency with our input. Previous studies have indicated that the signal quality of CSI Ratio is superior to the conjugation multiplication of CSI [34], [35], [39]. It should be noted that Widar2.0 provides an estimation of the target's position using multidimensional information. To enable a standardized comparison between SigCan and Widar2.0, we still use distance estimation error. Utilizing the estimated position provided by Widar2.0, we calculate the distance from this estimated position to the device, subsequently comparing this distance with the actual distance.

C. Indoor Environment

We now evaluate the effectiveness of the metrics for identifying interfering dynamic multipath. First, we analyze the

relationship between the performance of the metrics and estimation accuracy. Next, we remove the furniture, which may introduce powerful interfering dynamic multipath, and observe whether the metrics change accordingly.

We also compare the distance estimation accuracy of SigCan with a baseline approach (i.e., Widar2.0) at these positions across diverse indoor environments.

1) Relationship Between Metrics and Estimation Accuracy. Experimental Setting: We first conducted experiments in meeting room 1, as shown in Fig. 9(a). The distance between the devices was set to 10 cm, with a sampling rate of 500 Hz and a bandwidth of 20 MHz. The devices were positioned at chest height. 16 positions were chosen, as indicated in Fig. 9(a), with each position spaced at 1-meter intervals. Areas not covered by the photograph are represented with dashed black lines. Subjects stood at these positions and made slight body movements. In meeting room 2, a similar experiment was replicated. We select 14 positions near the table, as shown in Fig. 9(b). Positions were spaced at approximately 0.5-meter intervals along each line. Areas not covered by the photograph are represented with dashed orange lines. Subjects stood still at various locations and kept breathing. Data was collected for 10 seconds in each experiment.

Experiment Result When Metrics Indicate Multipath Cancellation: As shown in Fig. 10(a), we depict the distance estimation errors at various positions on a two-dimensional plane. We set the midpoint of the transceivers as the coordinate origin, with the front of the device aligned with the y-axis (corresponding to the aisle direction). It's apparent from the figure that around 93.75% of the tested positions can be estimated reliably. For positions classified as reliable by our metric, the average distance estimation error was 20.38 cm, with a median error of 20.21 cm. As shown in Fig. 11(a), we also present the mean distance estimation errors for different positions, comparing SigCan with Widar2.0. The error achieved by our method is significantly lower than that of Widar2.0 whose mean distance estimation error is 1.001 m.

Fig. 10(b) shows that around 92.86% of the tested positions can be estimated reliably with an average distance estimation error was 21.82 cm and a median error of 21.35 cm. Similarly, as shown in Fig. 11(b), we also present the mean distance estimation errors for different positions, comparing SigCan with Widar2.0 in the second meeting room. The error achieved by our method is significantly lower than that of Widar2.0 whose mean distance estimation error is 0.9169 m.

By merging data from both complex scenarios, we achieved reliable estimations for over 93% of positions. The average distance estimation error across all data points amounted to 21.05 cm, with a median error of 20.87 cm. In comparison, Widar2.0 achieve a mean error of 100.1 cm and 91.69 cm, respectively. Even considering Widar2.0's claimed median error of 0.75 m in their paper [9], our system still demonstrates a 50% reduction in error.

Experiment Result When Metrics Indicate Strong Dynamic Multipath: According to the value of the metrics, we divided the distance estimation errors into two categories: errors corresponding to dynamic multipath cancellation (reliable estimation) and errors corresponding to powerful dynamic multipath (unreliable estimation).

TABLE I
ESTIMATION ERROR IN COMPLEX INDOOR SCENARIO UNDER DIFFERENT CONFIDENCE

Estimation Confidence	Meeting Room	Median Estimation Error
Reliable Estimation	1	20.21 cm
Unreliable Estimation	1	79.10 cm
Reliable Estimation	2	21.35 cm
Unreliable Estimation	2	84.45 cm

The algorithm cannot consistently find the ideal CSI undergoing dynamic multipath cancellation, such as position 16 in Meeting Room 1 and Position 1 in Meeting Room 2. Therefore, as shown in Table I, the estimation error is larger at these positions. It also demonstrates that the performance of the signal on the metrics are able to indicate the condition of interfering dynamic multipath.

2) Relationship Between Metrics and Dynamic Multipath. Experimental Setting: To further validate that dynamic multipath affects the performance of metrics, we conducted the following experiments. We observed that there were reflectors, such as metal cabinets and electronic screens, near the positions with unreliable estimates. The receiver captures signals not only directly reflected from the target but also those bouncing off the human body and subsequently off the metallic furniture, leading to dynamic multipath interference. To validate the influence of furniture on dynamic multipath interference, and thereby the influence of dynamic multipath on the metrics, we repeated the experiments after removing the furniture from the environment while keeping other setups unchanged.

Experiment Result: After removing the furniture, the average distance estimation error in meeting room 1 diminished to 19.56 cm, displaying a median error of 10.39 cm. In meeting room 2, the average distance estimation error was 22.97 cm, with a median error of 21.32 cm. It is evident that the reflectors in the environment introduce dynamic multipath components when subjects are located near them, which can be indicated by the metrics proposed in Section VI.

D. Outdoor Environment

We have demonstrated the effectiveness of metrics for dealing with interfering dynamic multipath. Now, we assess the effectiveness of our method for handling with static multipath and noise. For convenience, we test the performance of SigCan in outdoor environments under various static multipath conditions and noise levels.

1) Distance Estimation Accuracy and Maximum Sensing Range. Experimental Setting: We conducted experiments in an outdoor square. As illustrated in Fig. 12, the distance between the transmitter (Tx) and receiver (Rx) (i.e., the length of the line of sight) is 1 m. The height of the device is equal to the subject's chest height. The bandwidth is 20 MHz, and the sampling rate is 500 Hz. Subjects stood at various locations along a line perpendicular to the line connecting the two devices, maintaining slight body movements. The subjects' distances from the device ranged from 10 meters to 20 meters. Data was

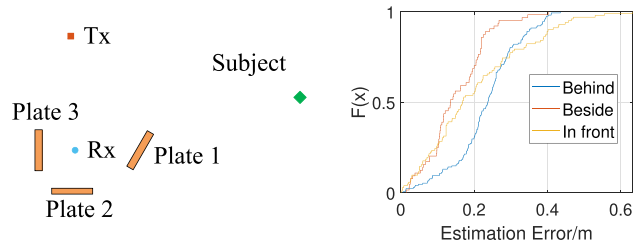

(a) Positions of WiFi transceivers, plate, and the subject. (b) Distance estimation error under different static multiple scenarios.

Fig. 13. Distance Estimation Accuracy under Different Static Multipath Scenarios.

collected for 10 seconds. We measured the actual distance using a laser range finder and simultaneously estimated the subjects' distances using the WiFi devices.

Experiment Result: From Fig. 12(b), it is apparent that the sensing range can extend up to 20 meters. Within this 20-meter range, the average estimation error is 15.36 cm, and the median error is 12.38 cm, demonstrating the accuracy of distance estimation even under low signal-to-noise ratio conditions, such as when subjects stand 20 meters away from the devices.

2) Impact of More Static Multipath. Experimental Setting: We now demonstrate the method's effectiveness in handling scenarios with increased static multipath. Subjects stand at various positions ranging from 3 m to 6 m away from the device. Then, we introduced 1 m $\times$ 1 m metal plates as powerful reflectors around the devices. Fig. 13 illustrates the locations of the metal plates in three positions, each 1 m away from the receiver (Rx). We maintained all other experimental conditions identical to those in Section VIII-D1.

Experiment Result: As shown in Fig. 13, following the introduction of the metal plates, the average estimation error was 23.22 cm, 15.03 cm, and 20.23 cm respectively, with a median estimation error of 23.7 cm, 13.53 cm, and 16.81 cm. This showed no significant change compared to the conditions without the metal plates, indicating that the algorithm can effectively handle static multipath without affecting the system's estimation accuracy.

3) Impact of Bandwidth. Experimental Setting: Now we investigate the impact of bandwidth. Subjects stand at various positions ranging from 10 meters to 17 meters away from the device. Subjects maintain their positions throughout subsequent experiments unless stated otherwise. We gradually decreased the bandwidth by selecting subcarriers with smaller frequency intervals, specifically 20 MHz, 10 MHz, and 4 MHz. All other conditions remain consistent with the experiment described in Section VIII-D1.

Experiment Result: Upon reducing the bandwidth, we discovered that even with bandwidth as small as 4 MHz, we could still estimate the target's distance with a mean estimation error of 1.04 m and a median error of 78.9 cm as shown in Fig. 14. The mean estimation error and median estimation error under a bandwidth of 10 MHz were 50.52 cm and 39.6 cm respectively.

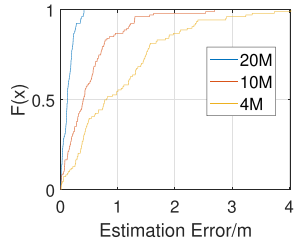

Fig. 14. Comparison with different bandwidths.

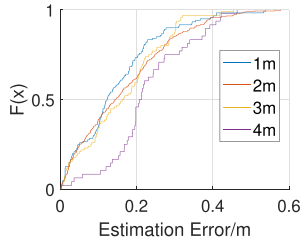

Fig. 15. Comparison with different LoS lengths.

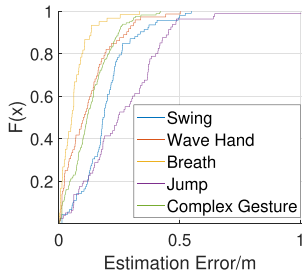

Fig. 16. Comparison with different motions.

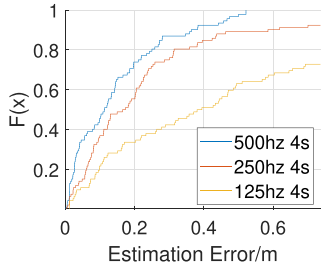

Fig. 17. Comparison with different sampling rates.

4) Impact of Different Lengths of LoS. Experimental Setting: We adjusted the length of Line-of-Sight (LoS) to 1 m, 2 m, 3 m, and 4 m, while keeping all other conditions consistent with the experiment in Section VIII-D1. Subsequently, we monitored the variation in errors.

Experiment Result: Fig. 15 illustrates the estimation errors corresponding to each LoS distances. For each LoS distance, the average estimation error was 14.63 cm, 16.49 cm, 16.29 cm, and 22.9 cm, with a median error of 12.26 cm, 14.41 cm, 16.44 cm, and 21.02 cm. We observed that even with an increased LoS distance of up to 4 meters, there was no substantial increase

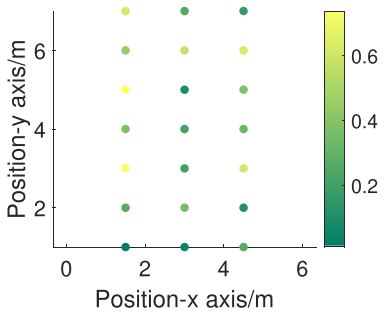

Fig. 18. Comparison with different positions. It should be noted that the error is the path length estimation error rather than the distance estimation error.

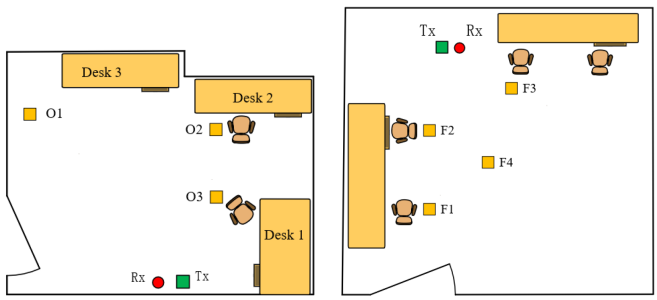

(a) Experiment setting of office 1. (b) Experiment setting of office 2.

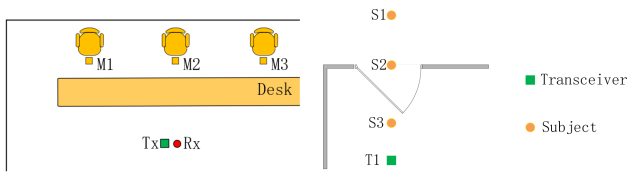

(c) Experiment setting of meeting room. (d) Experiment setting near the door.

Fig. 19. Case study experiment setting.

in estimation errors. The result suggests that the length of LoS doesn't significantly affect accuracy.

5) Impact of Sampling Rate. Experimental Setting: Given that SigCan relies on multiple samples to mitigate the impact of noise, we evaluate its effect by reducing the sampling rate. We downsample the collected data to simulate different sampling rates: 500 Hz, 250 Hz, and 125 Hz. All other conditions remain consistent with the experiment described in Section VIII-D1.

Experiment Result: As depicted in Fig. 17, we presented the variations in estimation errors for different sampling rates. It is evident that within the range of 500 Hz to 250 Hz, the algorithm demonstrated a high degree of estimation accuracy. The average error with 250 Hz was 40.34 cm, with a median error of 16.92 cm. A lower sampling rate results in increased distance estimation errors because noise has a more pronounced impact on the estimation process.

6) Impact of Motion. Experimental Setting: We now evaluate the impact of motion. Subjects were instructed to sway, wave their hand, breathe, jump, and perform gestures at each position. All other conditions remain consistent with the experiment described in Section VIII-D1.

Experiment Result: As illustrated in Fig. 16, it is evident that the algorithm demonstrated a high degree of estimation accuracy for several tested movements. The average error was 19.66 cm, 12.24 cm, 6.35 cm, 26.65 cm, and 13.06 cm for swaying, waving hand, breathing, jumping, and complex gestures (waving two hands simultaneously), respectively. This implies that this approach is suitable for a broad spectrum of common movements when conducting distance estimation.

7) Impact of Position: To comprehensively assess SigCan's performance across various positions relative to the devices, we conducted tests to evaluate its estimation capabilities away from the centerline.

Experimental Setting: We set the LoS length as 6 m and relocated subjects to positions situated outside the centerline while maintaining all other experimental conditions unaltered compared with conditions in Section VIII-D1. As the distance between the subject and Tx may not equal the distance between the subject and Rx, we calculate the estimation error by taking the difference between the actual and estimated propagation path length. Since the error analysis approach differs, the distance estimation errors in this section will naturally be larger than the estimation errors discussed in the previous section. These errors are solely utilized for analyzing variations in errors under different positions.

Experiment Result: On a 2D plane, we marked the coordinates of the transmitter and receiver devices as well as the target's actual position as shown in Fig. 18. We used the LoS connecting the Tx and Rx as the x-axis and the perpendicular bisector as the y-axis. Therefore, the coordinates of the Tx and Rx devices are $(-3\text{ m}, 0\text{ m})$ and $(3\text{ m}, 0\text{ m})$ respectively. The subject's position is indicated on the graph, and the depth of color represents the estimation error of the propagation path length. Within a certain range around the devices, the algorithm demonstrated a high degree of estimation accuracy. The average error was 35.04 cm in propagation path length, with a standard deviation of 22.43 cm and a median error of 32.66 cm, indicating that this work can provide reasonably accurate distance estimations across a substantial area around the devices.

E. Real-Time System

We built a real-time system with Matlab and tested its feasibility in real-world scenarios.

Experimental Setting: We tested the system in various environments as shown in Fig. 19(a), (b), (c), and (d). We selected locations frequently occupied in daily life, such as behind a desk, beside a chair, in a hallway, in a room corner, and near the door. The subject was asked to stand in these positions for a while and then move to the next location one by one. Meanwhile, every 10 seconds, SigCan used the collected data with a sampling rate of 500 Hz to estimate the distance.

Experiment Result: The average execution time on Intel Xeon W-10855M CPU for 10 seconds of input data is 3.29 s, satisfying real-time demands. When users performed in-place activities at the positions shown in Fig. 19(a), (b), and (c), the system periodically calculated metrics to determine whether a reliable distance estimation could be obtained from the signals. If a

TABLE II
ESTIMATION RESULT WITH THE DOOR OPEN/CLOSE

Pos of Subject	Pos of Device	Door Status	Subject-Device Distance	Average Estimation Distance
S1	T1	Close	2.3 m	2.61 m
S1	T1	Open	2.3 m	2.24 m
S2	T1	Open	1.5 m	1.23 m
S3	T1	Close	0.6 m	0.70 m
S3	T1	Open	0.6 m	0.77 m

reliable estimate could be provided, the system would output the distance estimation result. For each environment, we aggregated multiple reliable estimates from various users at various positions. The mean distance estimation errors for the meeting room, office 1, and office 2 are 26.68 cm, 24.74 cm, and 25.24 cm respectively. The results demonstrate the system's usability in real-world environments.

We specifically evaluated whether the estimation error would be affected by the door. We compare the two cases of door opening and door closing when subjects stand at different positions as shown in Fig. 19(d), and the error is shown in Table II. When a person is outside the door, closing and opening the door have some impact on the estimation results. However, even with the door closed, the sensing range of SigCan still exceeds the distance from the device to the door. This discrepancy in the estimation error does not lead to substantial misjudgments, hence not significantly affecting the intrusion detection.

IX. Discussion and Limitation

In this section, we discuss the limitations of the system and the potential direction of our future work.

Extension to multiple targets: Our framework focuses on estimating the ToF of a single target. If there are multiple targets, we envision that we can combine the beamforming with our work for multi-target ToF estimation. We can make the signal focus on the given direction and judge whether there are persons and how far the person is. Then we steer the beam direction of the signal and scan the environment.

Positions without reliable estimation: When the target is located at certain positions, such as household appliances mentioned in the experiment, the algorithm cannot consistently find the ideal CSI with minimal multipath effects from spatial and frequency diversity. Consequently, providing reliable estimation results becomes difficult in such cases. Exploring whether narrow bandwidths could potentially address this issue is an avenue we consider for future work.

X. Conclusion

ToF is a fundamental and key parameter in WiFi sensing applications, together with AoA and Doppler velocity. Traditionally ToF estimation of a moving target is considered very challenging because of the limited bandwidth of WiFi devices and the multipath effect in indoor environments, making ToF estimation unreliable. In this paper, we developed a novel phase difference based method to estimate the ToF of a moving target in multipath-rich indoor environments. By canceling the static multipath signals and quantifying the nulling degree of interfering dynamic multipath signals using time diversity, frequency diversity and space diversity, we could separate the reflected target path from the complex multipath and extract the ToF accurately and reliably. By implementing the method into the SigCan and evaluating it in different scenarios, we achieve a 50% decrease in ToF estimation error compared to state-of-the-art method. We envision that SigCan represents a significant step in making ToF estimation applicable to real-world WiFi sensing applications.

References

[1] Y.-H. Su, C. J. Yang, E. Hwang, and A. P. Sample, "Single packet, single channel, switched antenna array for RF localization," in *Proc. A CM Interact. Mobile Wearable Ubiquitous Technol.*, vol. 7, no. 2, Jun 2023, Art. no. 76, doi: 10.1145/3596263.

[2] W. Gong and J. Liu, "SiFi: Pushing the limit of time-based WiFi localization using a single commodity access point," in *Proc. A CM Interact. Mobile Wearable Ubiquitous Technol.*, vol. 2, no. 1, Mar. 2018, Art. no. 10, doi: 10.1145/3191742.

[3] C. Gentner, M. Ulmschneider, I. Kuehner, and A. Dammann, "WiFi-RTT indoor positioning," in *Proc. 2020 IEEE/ION Position Location Navigation Symp.*, 2020, pp. 1029–1035.

[4] K. Han, S. M. Yu, S.-L. Kim, and S.-W. Ko, "Exploiting user mobility for WiFi RTT positioning: A geometric approach," *IEEE Internet Things J.*, vol. 8, no. 19, pp. 14589–14606, Oct. 2021.

[5] X. Zhang, D. Zhang, Y. Xie, D. Wu, Y. Li, and D. Zhang, "Waffle: A waterproof mmwave-based human sensing system inside bathrooms with running water," in *Proc. A CM Interact. Mob. Wearable Ubiquitous Technol.*, vol. 7, no. 4, jan 2024. [Online]. Available: https://doi.org/10.1145/3631458

[6] D. Zhang et al., "LT-Fall: The design and implementation of a life-threatening fall detection and alarming system," in *Proc. A CM Interact. Mobble Wearable Ubiquitous Technol.*, vol. 7, no. 1, Mar. 2023, Art. no. 40, doi: 10.1145/3580835.

[7] D. Vasisht, S. Kumar, and D. Katabi, "Decimeter-level localization with a single WiFi access point," in *Proc. 13th USENIX Symp. Networked Syst. Des. Implementation*, 2016, pp. 165–178.

[8] Y. Xie, J. Xiong, M. Li, and K. Jamieson, "mD-track: Leveraging multi-dimensionality for passive indoor Wi-Fi tracking," in *Proc. 25th Annu. Int. Conf. Mobile Comput. Netw.*, 2019, pp. 1–16.

[9] K. Qian, C. Wu, Y. Zhang, G. Zhang, Z. Yang, and Y. Liu, "Widar2. 0: Passive human tracking with a single Wi-Fi link," in *Proc. 16th Annu. Int. Conf. Mobile Syst. Appl. Serv.*, 2018, pp. 350–361.

[10] X. Li et al., "Indotrack: Device-free indoor human tracking with commodity Wi-Fi," in *Proc. A CM Interact. Mobile Wearable Ubiquitous Technol.*, vol. 1, no. 3, Sep. 2017, Art. no. 72, doi: 10.1145/3130940.

[11] W. Li et al., "WiFi-CSI difference paradigm: Achieving efficient doppler speed estimation for passive tracking," in *Proc. A CM Interact. Mobile Wearable Ubiquitous Technol.*, vol. 8, no. 2, May 2024, Art. no. 63, doi: 10.1145/3659608.

[12] Y. Li et al., "Diversense: Maximizing Wi-Fi sensing range leveraging signal diversity," in *Proc. A CM Interactive Mobile Wearable Ubiquitous Technol.*, vol. 6, no. 2, pp. 1–28, 2022.

[13] Y. Xie, Z. Li, and M. Li, "Precise power delay profiling with commodity Wi-Fi," *IEEE Trans. Mobile Comput.*, vol. 18, no. 6, pp. 1342–1355, Jun. 2019.

[14] H. Wang et al., "MFDL: A multicarrier fresnel penetration model based device-free localization system leveraging commodity Wi-Fi cards," 2017, *arXiv: 1707.07514*.

[15] IEEE Standard for Information Technology–Telecommunications and Information Exchange Between Systems–Local and Metropolitan Area Networks–Specific Requirements Part 11: Wireless Lan Medium Access Control (MAC) and Physical Layer (PHY) Specifications Amendment 10: Mesh Networking, IEEE P802.11s/D8.0, Dec. 2010.

[16] J. Xiong, K. Sundaresan, and K. Jamieson, "Tonetrack: Leveraging frequency-agile radios for time-based indoor wireless localization," in *Proc. 21st Annu. Int. Conf. Mobile Comput. Netw.*, 2015, pp. 537–549.

[17] J. Xiong, K. Jamieson, and K. Sundaresan, "Synchronicity: Pushing the envelope of fine-grained localization with distributed MIMO," in *Proc. 1st A CM Workshop Hot Topics Wireless*, 2014, pp. 43–48.

[18] M. Kotaru, K. Joshi, D. Bharadia, and S. Katti, "SpotFi: Decimeter level localization using WiFi," in *Proc. 2015 A CM Conf. Special Int. Group Data Commun.*, 2015, pp. 269–282.

[19] K. Joshi, D. Bharadia, M. Kotaru, and S. Katti, "{WiDeo}: Fine-grained device-free motion tracing using RF backscatter," in *Proc. 12th USENIX Symp. Networked Syst. Des. Implementation*, 2015, pp. 189–204.

[20] X. Zhang, L. Chen, M. Feng, and T. Jiang, "Toward reliable non-line-of-sight localization using multipath reflections," in *Proc. A CM Interactive, Mobile, Wearable Ubiquitous Technol.*, vol. 6, no. 1, pp. 1–25, 2022.

[21] D. Zhang, H. Wang, and D. Wu, "Toward centimeter-scale human activity sensing with Wi-Fi signals," *Computer*, vol. 50, no. 1, pp. 48–57, 2017.

[22] H. Wang et al., "Human respiration detection with commodity WiFi devices: Do user location and body orientation matter?," in *Proc. ACM Int. Joint Conf. Pervasive Ubiquitous Comput.*, 2016, pp. 25–36.

[23] W. Wang, A. X. Liu, M. Shahzad, K. Ling, and S. Lu, "Understanding and modeling of WiFi signal based human activity recognition," in *Proc. 21st Annu. Int. Conf. Mobile Comput. Netw.*, 2015, pp. 65–76.

[24] J. Wang, J. Xiong, H. Jiang, X. Chen, and D. Fang, "D-watch: Embracing "bad" multipaths for device-free localization with cots RFID devices," *IEEE/A CM Trans. Netw.*, vol. 25, no. 6, pp. 3559–3572, 2017.

[25] J. Wang et al., "E-HIPA: An energy-efficient framework for high-precision multi-target-adaptive device-free localization," *IEEE Trans. Mobile Comput.*, vol. 16, no. 3, pp. 716–729, Mar. 2017.

[26] F. Zhang, C. Chen, B. Wang, and K. R. Liu, "WiSpeed: A statistical electromagnetic approach for device-free indoor speed estimation," *IEEE Internet Things J.*, vol. 5, no. 3, pp. 2163–2177, Jun. 2018.

[27] F. Zhang, C. Wu, B. Wang, H.-Q. Lai, Y. Han, and K. R. Liu, "WiDetect: Robust motion detection with a statistical electromagnetic model," in *Proc. A CM Interactive Mobile Wearable Ubiquitous Technol.*, vol. 3, no. 3, pp. 1–24, 2019.

[28] D. Halperin, W. Hu, A. Sheth, and D. Wetherall, "Tool release: Gathering 802.11n traces with channel state information," *Comput. Commun. Rev.*, vol. 41, no. 1, 2011, Art. no. 53, doi: 10.1145/1925861.1925870.

[29] D. Vasisht, S. Kumar, and D. Katabi, "Decimeter-level localization with a single WiFi access point," in *Proc. 13th USENIX Symp. Networked Syst. Des. Implementation*, Santa Clara, CA, USA, 2016, pp. 165–178. [Online]. Available: https://www.usenix.org/conference/nsdi16/technical-sessions/presentation/vasisht

[30] N. Yu, W. Wang, A. X. Liu, and L. Kong, "Qgesture: Quantifying gesture distance and direction with wifi signals," in *Proc. A CM Interactive, Mobile, Wearable Ubiquitous Technol.*, vol. 2, no. 1, pp. 1–23, 2018.

[31] D. Wu et al., "WiTraj: Robust indoor motion tracking with WiFi signals," *IEEE Trans. Mobile Comput.*, vol. 22, no. 5, pp. 3062–3078, May 2023.

[32] R. Gao et al., "Towards position-independent sensing for gesture recognition with Wi-Fi," in *Proc. A CM Interactive Mobile Wearable Ubiquitous Technol.*, vol. 5, no. 2, pp. 1–28, 2021.

[33] J. Zhang, Y. Li, H. Xiong, D. Dou, C. Miao, and D. Zhang, "HandGest: Hierarchical sensing for robust in-the-air handwriting recognition with commodity WiFi Devices," *IEEE Internet Things J.*, vol. 9, no. 19, pp. 19529–19544, Oct. 2022.

[34] Y. Zeng, D. Wu, J. Xiong, J. Liu, Z. Liu, and D. Zhang, "Multisense: Enabling multi-person respiration sensing with commodity WiFi," in *Proc. A CM Interact. Mob. Wearable Ubiquitous Technol.*, vol. 4, no. 3, pp. 102:1–102:29, 2020, doi: 10.1145/3411816.

[35] Y. Zeng, D. Wu, J. Xiong, E. Yi, R. Gao, and D. Zhang, "Farsense: Pushing the range limit of WiFi-based respiration sensing with CSI ratio of two antennas," in *Proc. A CM Interactive Mobile, Wearable Ubiquitous Technol.*, vol. 3, no. 3, pp. 1–26, 2019.

[36] D. Wu et al., "Fingerdraw: Sub-wavelength level finger motion tracking with WiFi signals," in *Proc. A CM Interactive Mobile Wearable Ubiquitous Technol.*, vol. 4, no. 1, pp. 1–27, 2020.

[37] Y. Liu et al., "Unifi: A unified framework for generalizable gesture recognition with Wi-Fi signals using consistency-guided multi-view networks," in *Proc. A CM Interact. Mob. Wearable Ubiquitous Technol.*, vol. 7, no. 4, Jan. 2024, Art. no. 168. [Online]. Available: https://doi.org/10.1145/3631429

[38] D. Halperin, W. Hu, A. Sheth, and D. Wetherall, "Tool release: Gathering 802.11 n traces with channel state information," *A CM SIGCOMM Comput. Commun. Rev.*, vol. 41, no. 1, pp. 53–53, 2011.

[39] Y. Zeng, D. Wu, R. Gao, T. Gu, and D. Zhang, "Fullbreathe: Full human respiration detection exploiting complementarity of CSI phase and amplitude of wifi signals," in *Proc. A CM Interact. Mob. Wearable Ubiquitous Technol.*, vol. 2, no. 3, pp. 148:1–148:19, 2018. doi: 10.1145/3264958.

Yang Li received the BEng degree from the School of Software, Northwestern Polytechnical University, in 2020. He is currently working toward the PhD degree in computer software and theory with the School of Computer Science, Peking University, Beijing, China. His research interests include wireless sensing and mobile computing.

Dan Wu received the PhD degree in computer science from Peking University, in 2020. He is currently a researcher with the Advanced Institude of Information Technology and the School of Computer Science, Peking University. His research interests include wireless sensing and mobile computing.

Jiahe Chen is currently working toward the undergraduate degree majoring in electronic information engineering with the School of Electronics Engineering and Computer Science, Peking University. His research interests include wireless sensing and mobile computing.

Weiyan Shi received the BEng and MSc degrees in software engineering from the Beijing Institute of Technology, Peking University. She is currently working toward the PhD degree with the Singapore University of Technology and Design. Her research interests include human-computer interaction and ubiquitous computing.

Leye Wang (Member, IEEE) received the PhD degree in computer science from TELECOM SudParis and University Paris 6, France, in 2016. He was a postdoctoral researcher with the Hong Kong University of Science and Technology. He is currently an assistant professor with the Key Laboratory of High Confidence Software Technologies, Peking University, China, MOE, and the School of Computer Science, Peking University. His research interests include ubiquitous computing, mobile crowdsensing, and urban computing.

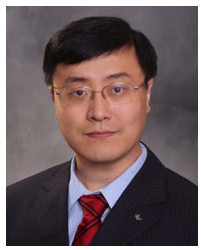

Lu Su (Member, IEEE) received the MS degree in statistics and PhD degree in computer science from the University of Illinois at Urbana-Champaign, in 2012 and 2013, respectively. He is an associate professor with the School of Electrical and Computer Engineering, Purdue University. His research interests include the general areas of Internet of Things and cyber-physical systems, with a current focus on wireless, mobile, and crowd sensing systems. He has also worked at IBM T. J. Watson Research Center and National Center for Supercomputing Applications. He has published more than 100 papers in referred journals and conferences, and serves as an associate editor of *A CM Transactions on Sensor Networks*. He is the recipient of NSF CAREER Award, University at Buffalo Young Investigator Award, ICCPS'17 best paper award, and the ICDCS'17 best student paper award.

Wenwei Li received the bachelor's degree in computer science and technology from the School of Electronics Engineering and Computer Science, Peking University, Beijing, China, in 2022. He is currently working toward the PhD degree in computer software and theory from the School of Computer Science, Peking University, Beijing, China. His current research interests include wireless sensing, cyber-physical systems, mobile computing, and deep learning.

Daqing Zhang (Fellow, IEEE) is a chair professor with the School of Computer Science, Peking University, China, and Telecom SudParis, IP Paris, France. His research interests include ubiquitous computing, mobile computing, big data analytics and AIoT. He has published more than 400 technical papers in leading conferences and journals, where his work on OWL-based context model and Fresnel Zone-based wireless sensing theory are widely accepted by pervasive computing, mobile computing and service computing communities. He was the winner of the Ten Years CoMoRea Impact Paper Award at IEEE PerCom 2013 and Ten Years Most Influential Paper Award at IEEE UIC 2019 and FCS 2023, the Best Paper Award Runner-up at A CM MobiCom 2022, UbiComp 2015 & 2016, the Distinguished Paper Award of IMWUT (UbiComp 2021), etc. He served as the general or program chair for more than a dozen of international conferences, and in the advisory board of Proceeding of A CM IMWUT.